THE PENNSYLVANIA STATE UNIVERSITY
SCHREYER HONORS COLLEGE

DEPARTMENT OF MEHANICAL AND NUCLEAR ENGINEERING

AN ANALYSIS OF A HYDROSTATIC BEARING

STUDENT NAME JUDY FAN
SPRING 2014

A thesis
submitted in partial fulfillment
of the requirements
for a baccalaureate degree
in Mechanical Engineering
with honors in Mechanical Engineering

Reviewed and approved* by the following:

Name: Gita Talmage
Title: Professor of Mechanical Engineering
Thesis Supervisor

Name: Domenic Santavicca
Title: Professor of Mechanical Engineering
Honors Adviser

* Signatures are on file in the Schreyer Honors College.

ABSTRACT

The focus of this thesis is on the analysis of hydrostatic bearings, in both one-dimension and two-dimensions, to establish their performance characteristics. One bearing configuration was analyzed analytically and numerically to determine the film thickness that minimizes the total energy loss. In two dimensions, for a specific bearing configuration, the pressure distribution was determined numerically, and the volumetric flow rate and load capacity were calculated. The flow rate and load capacity were found to vary linearly with increasing recess pressure and film thickness.

TABLE OF CONTENTS

LIST OF FIGURES

LIST OF TABLES

Chapter 1

Introduction

A bearing is used to minimize friction and to prevent contact between two surfaces, one of which is moving. Furthermore, some types of bearings are used to align machine components. For example, thrust bearings keep the shaft of rotating machinery axially aligned. There are essentially three types of bearings, with some overlap between each category: dry, fluid film and rolling element bearings (Hamrock, Jacobson & Schmid, 2004). Dry bearings are not lubricated, although they may employ a boundary lubricant, whereas fluid film and rolling element bearings are lubricated.

Bearing Classification

Dry bearings have two surfaces that rub together in either rolling or sliding motion. Fluid film bearings consist of two surfaces, one of which carries the load, separated by a lubricant film, either gas or liquid (Hamrock, Jacobson & Schmid, 2004). Journal and sleeve bearings are some of the common examples of fluid film bearings. Rolling element bearings, on the other hand, operate on the principle of rolling friction. These bearings are configured such that the two surfaces are separated from each other by rolling elements. The rolling elements, which are arranged between races, are typically balls, cylinder rollers, needle rollers, or barrel rollers. Roller bearings and ball bearings are among the common types of roller bearings. In general, rolling element bearings are more effective at reducing friction than fluid film bearings. However, fluid film bearings

are capable of operating at higher speeds than rolling element bearings (Hamrock, Jacobson & Schmid, 2004).

Lubrication in Bearing

A lubricant is any substance that reduces friction and wear; in addition, it provides smoother machine operation. Lubricants include liquids, gases, and greases, with greases used in rolling element bearings. Dry solids are also used as lubricants (Hamrock, Jacobson & Schmid, 2004). The characteristics of the lubricant are important in establishing the performance of any given bearing. The ways in which the lubricant is supplied to the bearing as well as the quantity of the lubricant also factor into the performance of a bearing. If no lubricant is supplied to, say a journal bearing, the shaft rubs against the bearing which results in high friction and wear, eventually leading to a bearing failure. If too much lubricant is fed into the bearing, a hydrostatic effect could result, possibly reducing the minimum film thickness, and thereby reducing the load (Hamrock, Jacobson & Schmid, 2004).

Fluid Film Bearing

Fluid film bearings support their loads on a thin layer of liquid or gas. Fluid film bearings are classified as hydrodynamic bearings or hydrostatic bearings. Hydrodynamic bearings have two surfaces, one of which is in motion, that are not parallel to each other. Therefore, to conserve mass, a pressure gradient in the direction of motion develops. It is this pressure gradient that supports the load. Hydrostatic bearings, however, are externally pressurized, and the lubricant is supplied from an external source, usually a pump (Booser & Khonsari, 2001). Hydrostatic bearings are chosen over other types of bearings due to their lower friction, higher load capacity at low speeds, higher reliability,

and longer life (Hamrock, Jacobson & Schmid, 2004). However, hydrostatic bearings usually involve more complex lubrication systems and have higher power consumption due to pumping losses (Booser & Khonsari, 2001). Similar to hydrodynamic bearings, hydrostatic bearings are normally in the form of thrust or journal bearings, carrying normal and radial loads, respectively.

Hydrostatic Bearing

The focus of this thesis is hydrostatic bearings, specifically on establishing a relation between pressure, film thickness, and load; and pressure, film thickness and flow rate. The pressure distribution within the bearing must be determined in order to establish the load. The operation of a hydrostatic bearing is illustrated in Figure 1. The lubricant is supplied from an external source. There is a pressure drop that develops between the lubricant source and the recess. In the figure, the lubricant flows into the recess, and then exits through the sides. The pressure distribution is also illustrated. The pressure is treated as uniform in the recess and decreases linearly to ambient pressure as the lubricant exits the bearing.

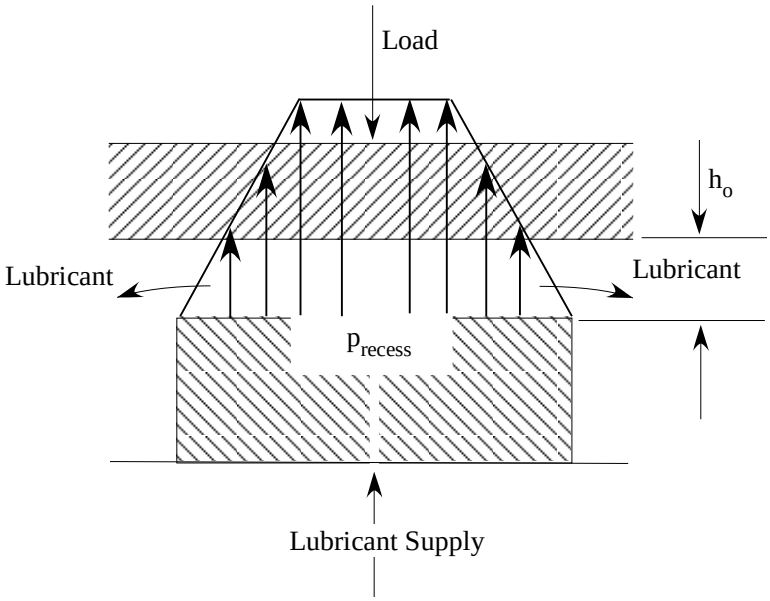

Figure 1. Schematic of a Bearing in Operation

The Reynolds equation is the key equation to obtain the pressure distribution seen in Figure 1. The two-dimensional (2D) Reynolds equation for a hydrostatic bearing is derived in Chapter 2. Chapter 3 contains a discussion of the one-dimensional (1D) problem, and in Chapter 4 the 1D analysis is extended to 2D. A conclusion of the work is presented in Chapter 5.

Chapter 2

The Derivation of Reynolds Equation

The derivation of the Reynolds equation is presented in this chapter. The derivation that is presented follows from five assumptions which are valid in many lubrication applications (Booser & Khonsari, 2001, p139-140). The five assumptions are:

1. The fluid is assumed to be Newtonian, where stress is directly proportional to the strain rate.
2. Inertia effects and body forces are assumed to be negligible compared to the viscous terms.
3. Variation of pressure across the film is assumed to be negligible.
4. Flow is laminar.
5. The curvature effects are negligible, implying that the thickness of the lubricant film is much smaller than the length or width of the bearing and allowing the use of Cartesian coordinate system.

The Navier-Stokes equations are:

$$\rho \frac{D\vec{v}}{Dt} = -\nabla P + \mu \nabla^2 \vec{u} + \rho \vec{F} \qquad (1.1)$$

With the five assumptions and the continuity equation, $\nabla \cdot \vec{u}=0$, the x component of the Navier-Stokes equations is:

$$\rho \left[u \frac{\partial u}{\partial x} + v \frac{\partial y}{\partial y} + w \frac{\partial w}{\partial z} \right] = -\frac{\partial P}{\partial x} + \mu \left[\frac{\partial^2 u}{\partial x^2} + \frac{\partial^2 u}{\partial y^2} + \frac{\partial^2 u}{\partial z^2} \right] \qquad (1.2)$$

In order to determine the significance of each term in the Navier-Stokes equations, these equations will be nondimensionalized with appropriate scaling, where "~" represents "on the order of." And U, L and h are known and W and P are unknown:

$$u, v \sim U$$

$$x, y \sim L$$

$$z \sim h$$

$$w \sim W$$

$$p \sim P$$

Applying the scales to Eq. (1.2),

$$\underbrace{\rho\left[u\frac{\partial u}{\partial x}+v\frac{\partial y}{\partial y}+w\frac{\partial w}{\partial z}\right]}_{\frac{\rho U^2}{L}} = \underbrace{-\frac{\partial P}{\partial x}}_{\frac{P}{L}} + \mu\left[\underbrace{\frac{\partial^2 u}{\partial x^2}+\frac{\partial^2 u}{\partial y^2}}_{\frac{\mu U^2}{L^2}} + \underbrace{\frac{\partial^2 u}{\partial z^2}}_{\frac{\mu U}{h^2}}\right] \qquad (1.3)$$

1 2 3 4

Divide Eq. (1.3) by $\frac{\mu U}{h^2}$ to obtain the following:

$$\text{Term 1} = \frac{\rho UL}{\mu}\left(\frac{h^2}{L^2}\right)$$

$$\text{Term 2} = \frac{Ph^2}{L\mu U}$$

$$\text{Term 3} = \frac{h^2 U}{L^2}$$

$$\text{Term 4} = 1$$

Because $\frac{h^2}{L^2} << 1$, term 3, $\frac{h^2 U}{L^2}$, is neglected, and two terms are left in Eq. (1.3): $\frac{Ph^2}{L\mu U}$ and 1. To balance the viscous effects $\frac{\partial P}{\partial x}$ must be on the order of 1, and the pressure scale for the nondimensionalization is $\frac{\mu UL}{h^2}$. Therefore, after nondimensionalization, Eq. (1.2) reduces to:

$$-\frac{\partial P}{\partial x} + \mu\frac{\partial^2 u}{\partial z^2} = 0 \qquad (1.4)$$

Similarly, the y-component of the Navier-Stokes equations reduces to:

$$-\frac{\partial P}{\partial y} + \mu\frac{\partial^2 v}{\partial z^2} = 0 \qquad (1.5)$$

Applying the nondimensionalization to the z-component of the Navier-Stokes equations reduces to:

$$\frac{\partial P}{\partial z} = 0 \qquad (1.6)$$

Equation (1.6) indicates that the pressure is not a function of the z, and the pressure is a function of x and y. To establish the x- and y-components of the velocity field, Eq. (1.4) and (1.5) are integrated twice. The x-component of the velocity that results after integrating Eq. (1.4) twice with respect to z is

$$u = \frac{z^2}{2\mu}\frac{\partial P}{\partial x} + c_1 z + c_2 \qquad (1.7)$$

The boundary conditions associated with Eq. (1.7) are:

$$z = 0,\ u(x,y,0) = 0$$

and

$$z = h,\ u(x,y,h) = 0.$$

Substituting c_1 and c_2 into Eq. (1.7), the velocity distribution in the x direction becomes:

$$u(x,y,z) = \frac{1}{2\mu}\frac{dp}{dx} z(z-h) \qquad (1.8)$$

Similarly, v(x,y,z) follows directly from u(z) with boundary condition:

$$z = 0,\ v(x,y,0) = 0$$

and

$$z = h,\ v(x,y,h) = 0.$$

The velocity distribution in the y direction, v(x,y,z), is obtained:

$$v(x,y,z) = \frac{1}{2\mu}\frac{dp}{dy} z(z-h) \qquad (1.9)$$

The Reynolds equation is needed in order to find the pressure distribution in fluid film, to obtain Reynolds equation, $\nabla\cdot\vec{u}=0$ is integrated with respect to the z from z = 0 to z = h:

$$\int_0^h \left(\frac{\partial u}{\partial x} + \frac{\partial v}{\partial y} + \frac{\partial w}{\partial z}\right)\, dz = 0$$

The plates are solid. Therefore, w(x,y,0) and w(x,y,h) are zero, which yields:

$$\int_0^h \left(\frac{\partial u}{\partial x} + \frac{\partial v}{\partial y}\right) dz = 0 \qquad (1.10)$$

Substituting Eqs.(1.8) and (1.9) into Eq. (1.10) and applying the Leibitz' rule yields:

$$\frac{1}{2\mu}\left[\frac{\partial^2 P}{\partial x^2} + \frac{\partial^2 P}{\partial y^2}\right]\int_0^h z(z-h)dz = 0$$

$$-\frac{h}{12\mu}\left[\frac{\partial^2 P}{\partial x^2} + \frac{\partial^2 P}{\partial y^2}\right] = 0$$

$$\left[\frac{\partial^2 P}{\partial x^2} + \frac{\partial^2 P}{\partial y^2}\right] = 0 \qquad (1.11)$$

Equation (1.11) is the 2D Reynolds equation that will be used to determine the pressure distribution in Chapter 3 and Chapter 4.

Chapter 3

Hydrostatic Bearing in One Dimension

The type of hydrostatic design used on many types of machinery and devices is described as an oil pad, as shown in Figure 2 below. An oil pad is used to eliminate internal friction. Load is introduced by a hydraulic cylinder to the bottom of the bearing loading block. As the shaft turns, the torque between the shaft and bearing is evaluated by measuring the force exerted against a scale that is placed at the end of the friction arm. A set of reliefs are set at the surface between the shoe and bearing holder when supplying high pressure oil. The two surfaces can be separated and the frictional drag can be reduced to zero (Fuller, 1956).

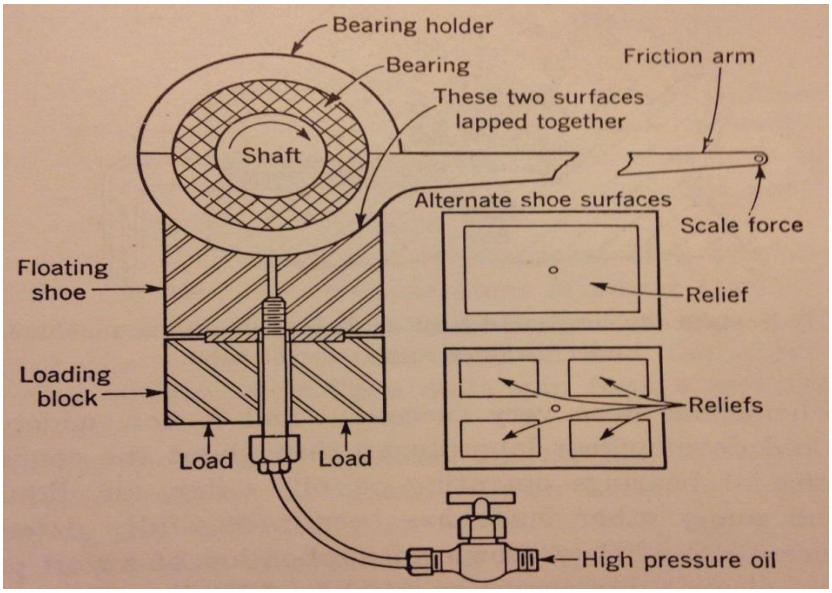

Figure 2. Hydrostatic lubrication as applied to bearing-testing machine. From Theory and Practice of Lubrication for Engineers by D. Fuller, 1956, page. 83

To optimize the bearing performance, the optimum film thickness that produces the minimum friction loss and pumping loss will be obtained. Figure 3 shows the top and front view of the bearing, where the top image in Figure 3 is the top view, and the bottom image in Figure 3 is the front view.

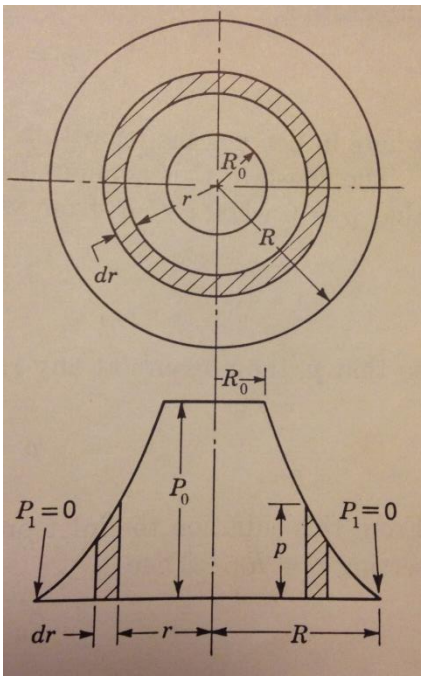

Figure 3. Plan view and radial pressure distribution of the hydrostatic step bearing. From Theory and Practice of Lubrication for Engineers by D. Fuller, 1956, page. 87

The geometry and property of the bearing used in this case are from example 11, page 89, of Theory and Practice of Lubrication for Engineers by Dudley Fuller:

R = 8 in, the shaft radius,

R_o= 5 in, the recess radius,

$\mu = 4.24x10^{-6}$ reyn, the viscosity,

P_o= 825 psig, the recess pressure,

b = 2πr, and b represents the width of the slot in Cartesian coordinates, and

L is the length of the slot in Cartesian coordinate.

The flow rate equation used in the 1D case is derived as follows:

$$Q = \int_0^h ub\, dz = \int_0^h \frac{1}{2\mu}\frac{dp}{dx} z(z-h)\, dz \qquad (2.1)$$

$$Q = -\frac{h^3}{12\mu}\frac{dp}{dx} b \qquad (2.2)$$

$$Q = \frac{\Delta P b h^3}{12\mu L} \qquad (2.3)$$

Equation (2.3) is in Cartesian coordinates. This result can be transform in to cylindrical coordinate by replacing b with 2πr, ΔP with dP, and L with dr:

$$Q = -\frac{dP 2\pi r h^3}{12\mu dr} \qquad (2.4)$$

The negative sign in Eq. (2.4) indicates that the pressure decreases radially outward. Integrating Eq. (2.4) yields

$$P(r) = -\frac{6\mu Q}{\pi h^3} \ln r + C \qquad (2.5)$$

Equation (2.5) is subject to the boundary condition that P (R_0) = 0, and C is determined to be:

$$C = \frac{6\mu Q}{\pi h^3} \ln R \qquad (2.6)$$

Substituting Eq. (2.6) into Eq. (2.5) pressure at any radius r is obtained,

$$P = -\frac{6\mu Q}{\pi h^3} \ln\left(\frac{R}{r}\right) \qquad (2.7)$$

In this particular case, the recess pressure, P_o, at recess radius, R_o, is substituted into Eq. (2.7). After rearranging the equation, the flow rate is determined to be:

$$Q = \frac{P_o \pi h^3}{6\mu \ln(\frac{R}{R_o})} \qquad (2.8)$$

Referring to Figure 1 in Chapter 1, the total load (W) can be evaluated as the sum of the forces exerted by the recess pressure over the rectangular recess area of radius R_o and the variable pressure P acting on the sill area of the bearing. The equation for load carrying capacity can be expressed as:

$$W = P_o\left(\pi {R_o}^2\right) + \int_{R_o}^{R} P(2\pi r)dr \qquad (3.1)$$

Substituting Eq. (2.7) into Eq. (3.1) results in:

$$W = P_o\left(\pi {R_o}^2\right) + \frac{12\mu Q}{h^3}\int_{R_o}^{R} \ln\left(\frac{R}{r}\right) rdr \qquad (3.2)$$

Substituting Q from Eq. (2.8), and integrating Eq. (3.2) yields,

$$W = \frac{P_o \pi}{2}\left[\frac{R^2 - {R_o}^2}{\ln\left(\frac{R}{R_o}\right)}\right] \qquad (3.3)$$

The optimum film thickness occurs when total energy loss is at its minimum. Total energy loss is the sum of the friction loss and pump work that is required to pump lubricant through the film space. Pump work in this case is a constant for a given flow rate and pressure difference; it is the work done to force out the lubricant, and can be expressed as:

$$E_p = Q(\Delta P) \qquad (4)$$

Friction loss can be found using the Newton's equation for friction drag,

$$F = \mu A \frac{v}{h} \qquad (5.1)$$

where A is the surface area, v is the velocity of the shaft rotation. The velocity of the shaft rotation can be replaced by $v = \omega r$, in which ω is the angular velocity and r is the radius. Taking the derivative of Eq. (5.1) yields

$$dF = \mu 2\pi r dr \frac{\omega r}{h} \qquad (5.2)$$

The torque in the film as a function of r is

$$dT = \mu 2\pi r dr \frac{\omega r}{h}(r) \tag{5.3}$$

$$T = \frac{2\mu\pi\omega}{h}\int_{R_o}^{R} r^3 dr \tag{5.4}$$

$$T = \frac{2\mu\pi\omega}{h}\left[\frac{R^4}{4} - \frac{{R_o}^4}{4}\right] \tag{5.5}$$

Friction loss is given by the relation:

$$E_f = \frac{2\pi TN}{60} \tag{5.6}$$

where N is the angular velocity, in rpm. Replace the angular velocity from Eq. (5.5) with $\frac{2\pi N}{60}$, and replace T in Eq. (5.6) with Eq. (5.5) to obtain:

$$E_f = \left(\frac{2\pi N}{60}\right)^2 \frac{2\mu\pi}{h}\left[\frac{R^4}{4} - \frac{{R_o}^4}{4}\right] \tag{5.7}$$

Figure 4 and Table 1 below show the effects of film thickness on pumping loss, friction loss and total energy loss. Figure 4 is in agreement with the published result (Fuller, 1956, p. 93). From the result, a film thickness of 0.004 in yields the optimum pump efficiency. Table 1 includes the numerical results of pumping loss, friction loss and total energy loss with film thickness varying from 0.001in to 0.009 in.

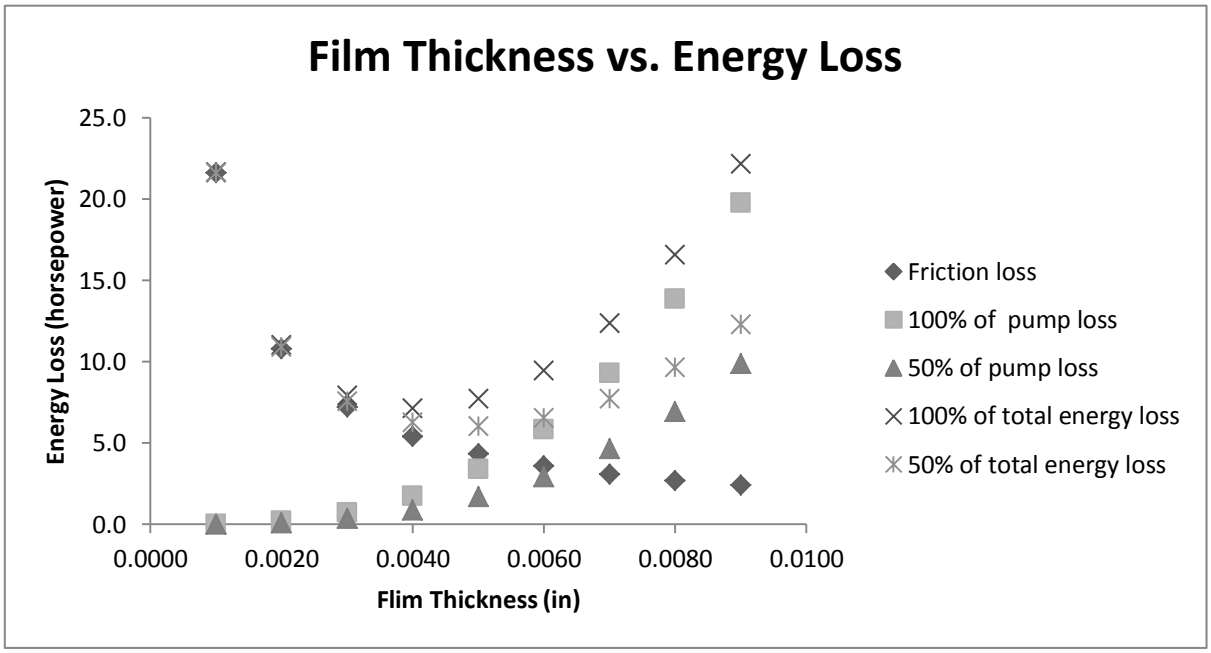

Figure 4. Film thickness vs. energy loss

Table 1. Film thickness, pump loss and friction loss

ho	E_f	E_p(100%)	E_p(50%)	E_total (100%)	E_total(50%)
0.0010	21.6071	0.0271	0.0135	21.6342	21.6207
0.0020	10.8036	0.2168	0.1084	11.0203	10.9119
0.0030	7.2024	0.7316	0.3658	7.9339	7.5681
0.0040	5.4018	1.7341	0.8670	7.1358	6.2688
0.0050	4.3214	3.3868	1.6934	7.7082	6.0148
0.0060	3.6012	5.8524	2.9262	9.4536	6.5274
0.0070	3.0867	9.2934	4.6467	12.3802	7.7335
0.0080	2.7009	13.8724	6.9362	16.5733	9.6371
0.0090	2.4008	19.7520	9.8760	22.1528	12.2768

Continuing with the same recess pressure, 825 psig, the 1D pressure distribution is found. In the 1D case, pressure varies in the x direction from 825 psig to 0 psig when x varies from 0 to L, L being the circumference of the journal, which in this case is 31.415 in. Viscosity is given to be $4.24\text{x}10^{-6}$ reyn in this particular example. The analytical

solution is found by integrating the 1D form of Eq. (1.11). Although an analytical solution exists for the 1D problem, it does not exist for the 2D problem. Therefore, to better understand the finite differences, the 1D problem will also be solved using finite differences. A 1D finite difference approximation to the Reynolds equation is made and compared to the analytical solution. To obtain a numerical solution of the 1D form of Eq. (1.11), a Taylor series expansion is taken (see Appendix A). The Taylor series expansion of $\frac{d^2P}{dx^2} = 0$ is:

$$\frac{P_{i+1} - 2P_i + P_{i-1}}{(\Delta x)^2} = 0 \qquad (6)$$

Figure 5 is the schematic of the 1D mesh that shows the coordinate used to obtain Eq. (6).

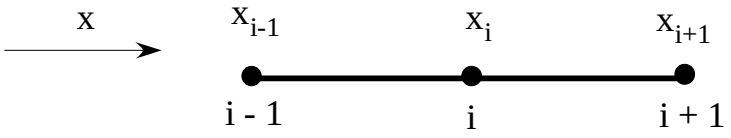

Figure 5. Schematic of the 1D mesh

Both analytical and numerical solutions of the pressure are solved using MATLAB, and the MATLAB codes are presented in Appendix B. The analytical and numerical results obtained appeared to be in excellent agreement. The pressure distribution is presented with ten nodes, with Δx being 3.142 in. Figure 6 is the pressure distribution plot comparing the analytical to the numerical solution, observe that pressure decreases linearly with x direction.

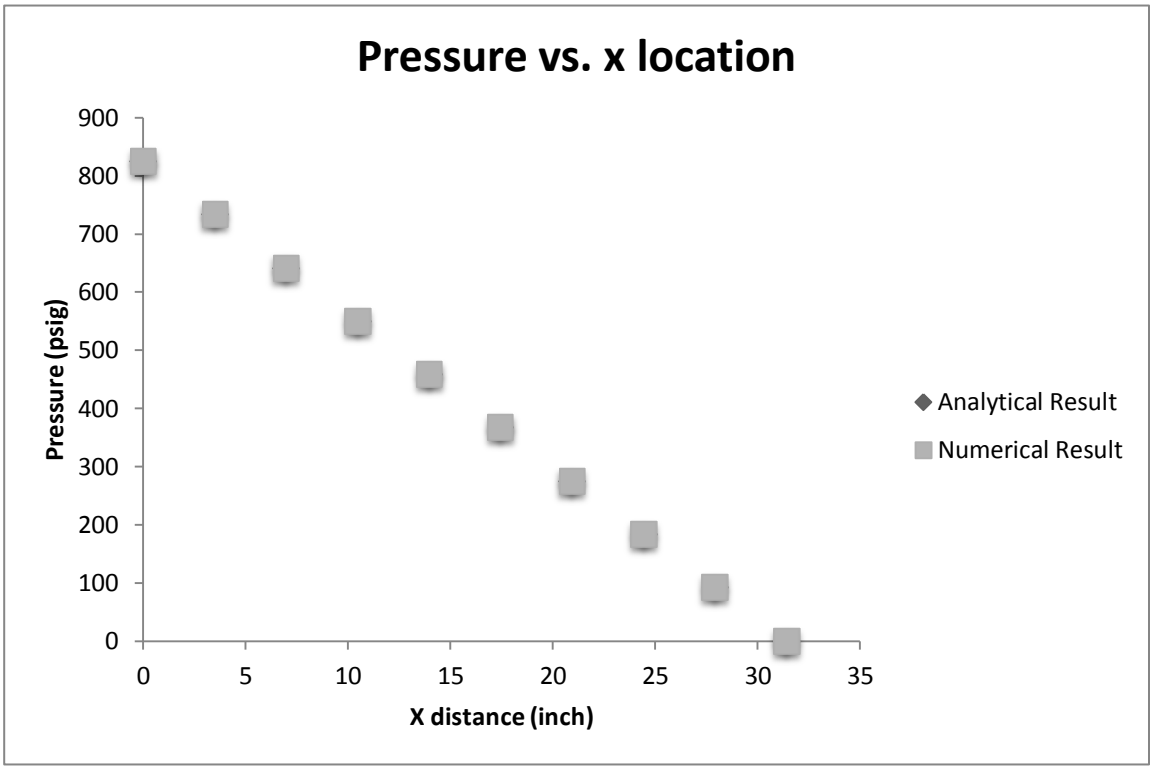

Figure 6. Pressure distribution in the x direction

Chapter 4

The Two Dimensional Hydrostatic Bearing

After analyzing the case in which pressure varies in only one dimension, an analysis with pressure varying in both x and y directions is carried out with the same parameters that were used in Chapter 3. In the 2D case, the geometry used is a bearing pad with length of 25 in and width of 20 in, see Figure 7.

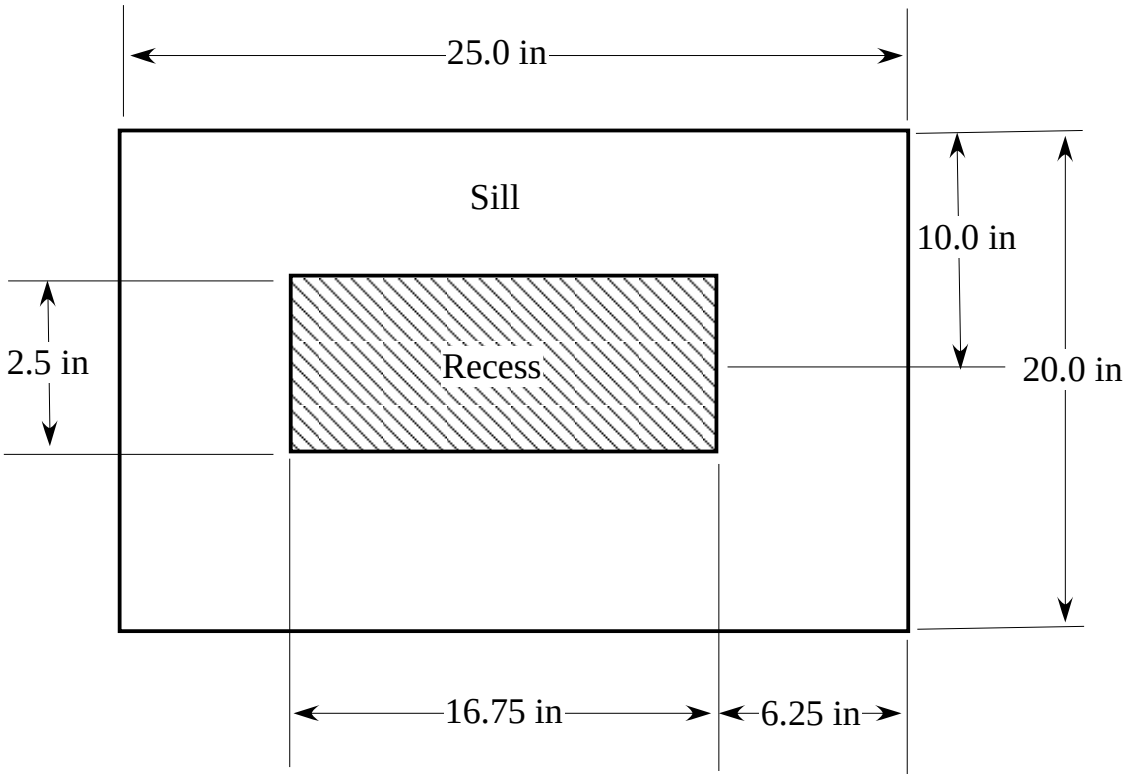

Figure 7. Schematic of the geometry used in the 2D case (not drawn in scale)

The recess area is a rectangle whose right side boundary is 6.25 in to the left of the right side of the bearing pad. The bottom of the recess area is 8.75 in above the

bottom of the bearing pad. The recess area has length (l_r) of 12.5 in and a width (w_r) of 2.5 in. The boundary conditions for this analysis are 0 psig along the boundaries of the bearing pad, and the recess pressure within and along the recess boundaries is 825 psig. Figure 8 is a schematic of outflow over the sill, where the flow rates through surfaces 2 and 4 are the same, and the flow rates through surfaces 1 and 3 are the same.

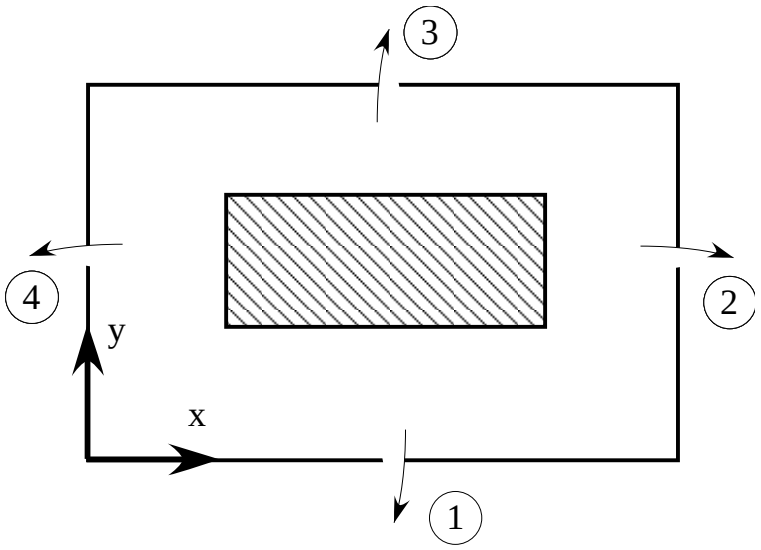

Figure 8. Schematic of outflow over sill surfaces

Flow rate and load capacity is calculated in MATLAB using equations that are derived as follows. From Chapter 2, the velocity distribution in the x direction is given by

$$u = \frac{1}{2\mu}\frac{dp}{dx}z(z-h) \qquad (1.8)$$

To obtain the flow rate through surfaces 2 and 4 in Figure 8, a double integration is performed on Eq. (1.8)

$$\int_0^w \int_0^h \frac{1}{2\mu}\frac{dp}{dx}z(z-h)dzdy \qquad (7.1)$$

In Eq. (7.1), h is the clearance height, and w is the width of the oil pad. Because the flow rate through surfaces 2 and 4 are the same, Q_x is twice Eq. (7.1). The flow rate in the x direction is found to be:

$$Q_x = -\frac{h^3}{12\mu}\frac{dp}{dx}w \qquad (7.2)$$

The y-component of the velocity distribution from Chapter 2, is:

$$v = \frac{1}{2\mu}\frac{dp}{dy}z(z-h) \qquad (1.9)$$

To determine the flow rate in the y direction, the same method of integration is performed on Eq. (1.9):

$$\int_0^L \int_0^h \frac{1}{2\mu}\frac{dp}{dy}z(z-h)dzdx \qquad (7.3)$$

where L is the length of the oil pad specified in Chapter 2. The flow rate in the y direction is found to be:

$$Q_y = -\frac{h^3}{12\mu}\frac{dp}{dy}L \qquad (7.4)$$

The total load capacity (W) is the sum of the load in the recess area and the load in the sill area. The load in the recess area is the recess pressure times the recess area:

$$W_{recess} = P_o l_r w_r \qquad (7.5)$$

Because pressure varies in the sill area, the load associated with the sill area is calculated by integration of the pressure over the sill area:

$$W_{sill} = \int_A P\,dxdy \qquad (7.6)$$

Therefore, the total load capacity is the sum of Eqs. (7.5) and (7.6):

$$W_{total} = P_o l_r w_r + \int_A P\,dxdy \qquad (7.7)$$

The pressure cannot be determined analytically in the 2D case. Therefore, it will be determined from the Reynolds equation, Eq. (1.11), using a finite difference approximation. Figure 9 shows a schematic of the 2D mesh used in solving the finite difference solution.

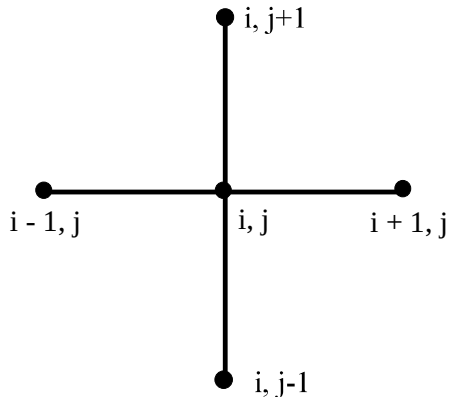

Figure 9. Schematic of the 2D mesh

The finite difference approximation to the Reynolds equation is given by

$$\frac{P_{i+1,j}-2P_{i,j}+P_{i-1,j}}{(\Delta x)^2}+\frac{P_{i,j+1}-2P_{i,j}+P_{i,j-1}}{(\Delta y)^2}=0 \qquad (8.1)$$

Equation (8.1) can be rearranged to determine $P_{i,j}$:

$$P_{i,j}=\frac{\frac{P_{i+1,j}+P_{i-1,j}}{(\Delta x)^2}+\frac{P_{i,j1,j}+P_{i,j-1}}{(\Delta y)^2}}{2(\frac{1}{(\Delta x)^2}+\frac{1}{(\Delta y)^2})} \qquad (8.2)$$

In terms of the finite difference approximation, the boundary condition on the pressure are:

$$j = 2, 3, \ldots, N-1, \quad P_{1,j} = P_{M,j} = 0$$

$$i = 1, 2, \ldots, M, \quad P_{i,N} = 0$$

$$i = 1, 2, \ldots M, \quad P_{1,j=}P_o$$

where M represents the number of nodes in the x direction, and N represents the number of nodes in the y direction.

In order to present a more accurate pressure distribution, appropriate coordinates within the bearing pad are developed. With 161 nodes in the x and y directions, the distance between each node in the x direction is 0.156 in and the distance between each node in the y direction is 0.125 in. The MATLAB code given in Appendix C. An iterative process was used to establish the pressure distribution. Using the MATLAB code, the pressure distribution is plotted in Figure 10 where the z axis is pressure, and x and y axes represent the x and y directions of the oil pad, respectively. As can be seen in Figure 10, the pressure peaks at 825 psig in the recess area and decreases to 0 psig at the boundaries of the oil pad. In addition to having a sufficient number of nodes within the oil pad, the number of iterations in MATLAB is also important in creating an accurate pressure distribution. The pressure distribution is obtained with 7000 iterations, in which the result converges with an error of $9.85x10^{-9}$. Similar to the 1D case, the finite difference solution is provided in Appendix D, in which the relationship between nodes in both x and y directions are derived.

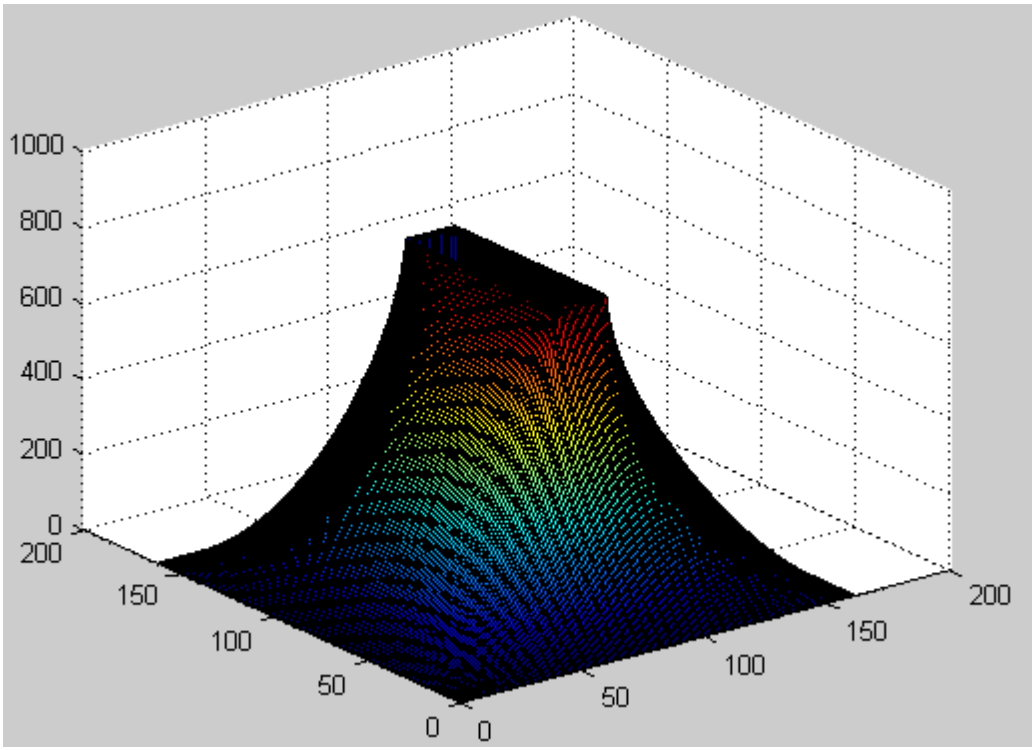

Figure 10. 2D pressure distribution of the oil pad

The numerical result obtained from MATLAB is used to compare with the experimental result obtained from Fuller. Equations used to calculate experimental values of the flow rate and load are:

$$Q = 0.488\ \frac{P_o h^3}{\mu} \qquad (8)$$

$$Load = 177.8 P_o \qquad (9)$$

With the parameter and properties given, the experimental result for flow rate is calculated to be 9.255 in^3/s, and the load is 146,685 lbf. With 7000 iteration, the numerical results obtained from MATLAB are: Q= 9.591in^3/s and W= 150,440 lbf. The percent difference between the numerical and experimental results are 3.63% for

flow rate and 2.56% for the load. These results are for a 161x161 mesh. In order to reduce the time to obtain results in MATLAB, an analysis with 81x81 mesh in both x and y direction is carried out using the same initial conditions. With an 81x81 mesh and a 7000 iterations, the numerical results obtained are as follows: Q = 9.838in^3/s and W = 148,930 lbf. The percent difference between the numerical and experimental result becomes 6.3% for flow rate and 1.53% for the load. The percent difference for flow rate almost doubled while that for the load decreased by about 1%. The experimental flow rate coefficient is 0.488, and the numerical flow coefficient is 0.5187. The experimental load coefficient is 177.8, whereas the numerical load coefficient is 180.52.

A complete numerical result, with an 81x81 mesh, is presented in Table 2 in which the recess pressure varies from 725 psig to 825 psig. The clearance height varies from 0.001 in to 0.009 in for the same recess pressures. The results in Table 2 show that for the same clearance, the flow rate increases when the recess pressure increases; at the same recess pressure, the flow rate also increases as clearance increases. On the other hand, the total load remains constant for the same recess pressure regardless of the clearance height but it increases with increasing recess pressure. Furthermore, the change in temperature of the fluid increases when recess pressure increases. However, ΔT is sufficiently small that the viscosity is essentially constant.

Table 2. Numerical results with varying recess pressure and clearance height

Po (psig)	h (in)	Q (in^3/s)	Flow rate Coefficient	Load (lbf)	Load Coefficient	E_p (horsepower)	ΔT (F)
725	0.001	0.009	0.516	130880	180.52	0.0009	5.06
725	0.003	0.233	0.519	130880	180.52	0.0256	5.06
725	0.005	1.081	0.519	130880	180.52	0.1187	5.06
725	0.007	2.965	0.519	130880	180.52	0.3257	5.06
725	0.009	6.303	0.519	130880	180.52	0.6923	5.06
750	0.001	0.009	0.519	135390	180.52	0.0010	5.23
750	0.003	0.242	0.519	135390	180.52	0.0274	5.23
750	0.005	1.118	0.519	135390	180.52	0.1270	5.23
750	0.007	3.068	0.519	135390	180.52	0.3486	5.23
750	0.009	6.520	0.519	135390	180.52	0.7409	5.23
775	0.001	0.009	0.519	139900	180.52	0.0011	5.41
775	0.003	0.250	0.519	139900	180.52	0.0293	5.41
775	0.005	1.155	0.519	139900	180.52	0.1356	5.41
775	0.007	3.170	0.519	139900	180.52	0.3722	5.41
775	0.009	6.737	0.519	139900	180.52	0.7911	5.41
800	0.001	0.010	0.519	144420	180.52	0.0012	5.58
800	0.003	0.258	0.519	144420	180.52	0.0312	5.58
800	0.005	1.193	0.519	144420	180.52	0.1445	5.58
800	0.007	3.272	0.519	144420	180.52	0.3966	5.58
800	0.009	6.955	0.519	144420	180.52	0.8430	5.58
825	0.001	0.010	0.519	148930	180.52	0.0012	5.76
825	0.003	0.266	0.519	148930	180.52	0.0332	5.76
825	0.005	1.230	0.519	148930	180.52	0.1537	5.76
825	0.007	3.374	0.519	148930	180.52	0.4218	5.76
825	0.009	7.172	0.519	148930	180.52	0.8965	5.76

Chapter 5

Conclusion

The work that was done to complete this thesis includes the derivation of the Reynolds equation, flow rate and load capacity for 1D and 2D cases. Using these equations, a 1D pressure distribution was obtained both analytically and numerically and a 2D pressure distribution was obtained numerically.

The analysis of the 1D pressure distribution showed that friction loss decreased as film thickness increases, whereas pumping loss increased with increasing film thickness. Furthermore, a film thickness of 0.004 in produced the minimum pumping and friction loss. After performing analytical and numerical analyses on the 1D problem, it was found that the analytical and numerical results are in excellent agreement and that pressure decreased linearly with increasing x.

The results obtained from the 2D analysis showed that the percent different between numerical and experimental results are 6.3% for flow rate and 1.53% for the load. In addition, they also showed that flow rate increased with increasing recess pressure, and load capacity also increased with increasing recess pressure. Viscosity can be considered constant due to the fact that temperature change was sufficiently small.

Appendix A

Finite difference solution for 1D case

$$P_{i+1} = P_i + \frac{dP_i}{dx}\Delta x + \frac{\mathrm{d}^2P}{dx^2}\frac{(\Delta x)^2}{2!} + \frac{d^3P}{dx^3}\frac{(\Delta x)^3}{2!} + \cdots \quad (10.1)$$

$$P_{i-1} = P_i - \frac{dP_i}{dx}\Delta x + \frac{d^2P}{dx^2}\frac{(\Delta x)^2}{2!} - \frac{d^3P}{dx^3}\frac{(\Delta x)^3}{2!} \pm \cdots \quad (10.2)$$

$$P_{i+1} + P_{i-1} = 2P_i + \frac{d^2P}{dx^2}(\Delta x)^2 + 2\frac{d^4P}{dx^4}\frac{(\Delta x)^4}{4!} + \cdots \quad (10.3)$$

At a point, Δxgoes to zero which means higher order term in Eq. (10.3) goes to zero as well

$$\frac{d^2P}{dx^2} = \frac{P_{i+1}-2P_i+P_{i-1}}{(\Delta x)^2} \quad (10.4)$$

From x component of the Reynolds equation, $\frac{d^2P}{dx^2} = 0$, Eq. (10.4) can be expressed as:

$$\frac{P_{i+1}-2P_i+P_{i-1}}{(\Delta x)^2} = 0 \quad (10.5)$$

Appendix B

MATLAB code for 1D analytical and numerical solutions

Numerical

```
clc; clear
x=(2*pi*5)/9;
X= x^2;

A = [1 0 0 0 0 0 0 0 0 0; 1/X -2/X 1/X 0 0 0 0 0 0 0; 0 1/X -2/X 1/X 0 0 0 0 0 0; 0 0 1/X -2/X 1/X 0 0 0 0 0; 0 0 0 1/X -2/X 1/X 0 0 0 0; 0 0 0 0 1/X -2/X 1/X 0 0 0; 0 0 0 0 0 1/X -2/X 1/X 0 0; 0 0 0 0 0 0 1/X -2/X 1/X 0; 0 0 0 0 0 0 0 1/X -2/X 1/X; 0 0 0 0 0 0 0 0 0 1]
B = [825; 0; 0; 0; 0; 0; 0; 0; 0; 0];
C = [1; 2; 3; 4; 5; 6 ; 7; 8; 9; 10];

D= mldivide(A,B)
plotmatrix(C,D);
grid on;
xlabel('X distance (in)');
ylabel('pressure (psi)');
```

Analytical

```
clc; clear

d= (2*pi*5)/9

x = 1: 1 : 10;
y = 825 * (1- ( d*(x-1) / (2*pi*5)));
A= [x; y]
plot (x,y);
grid on;
xlabel('X distnace (in)');
ylabel('pressure (psi)');
```

Appendix C
MATLAB code for two dimensional pressure distribution

```
clear;clc
%Length and width of the geometry
l=25;
w=20;
h=0.06;
u=435*10^-7;
l_r=12.5;
w_r=2.5;

%i_max abnd j_max
i_max=161;
j_max=161;

%i and j of the slit
i_slit_1= 20;
i_slit_2= 60;
j_slit_1= 35;
j_slit_2= 45;

%Input
p_o= 825;

p = zeros(i_max, j_max)

%Delta x and delta y
d_x= l/(i_max-1);
d_y= w/(j_max-1);

%Determine x(i) and y(j)
x(1)=0.0;
for i=2:i_max;
   x(i)= x(i-1)+ d_x;
end

y(1)=0.0;
for j=2:j_max;
   y(j)= y(j-1) + d_y;
end

%pressrue along the slit
```

```
for i= i_slit_1:i_slit_2;
   p(i,j_slit_1)= p_o;
end

for i= i_slit_1:i_slit_2;
   p(i,j_slit_2)=p_o;
end

for j= j_slit_1:j_slit_2;
   p(i_slit_1,j)= p_o;
end

for j=j_slit_1:j_slit_2;
   p(i_slit_2,j)=p_o;
end

%surf(p)
for j=1:j_max;
   for i = 1:i_max;
      prev_p(i,j)=p(i,j);
   end
end

%iteration
for k=1:7000;
%pressure in region 1
for j=2:j_slit_1-1;
   for i=2:i_max-1;
      t_x = ((p(i+1,j))+(p(i-1,j)))/((d_x)^2);
      t_y = ((p(i,j+1))+(p(i,j-1)))/((d_y)^2);
      denom = (2.)*((1./((d_x)^2)) + ((1./((d_y)^2))));


      p(i,j) = ((t_x+t_y)/denom);
  end
end

%pressure in region 2a and 2b

for j=j_slit_1:j_slit_2;
   for i= 2:i_slit_1-1;
      t_x = ((p(i+1,j))+(p(i-1,j)))/((d_x)^2);
      t_y = ((p(i,j+1))+(p(i,j-1)))/((d_y)^2);
      denom = (2.)*((1./((d_x)^2)) + ((1./((d_y)^2))));
```

```
        p(i,j) = ((t_x+t_y)/denom);
    end

    for i= i_slit_2+1:i_max-1;
        t_x = ((p(i+1,j))+(p(i-1,j)))/((d_x)^2);
        t_y = ((p(i,j+1))+(p(i,j-1)))/((d_y)^2);
        denom = (2.)*((1./((d_x)^2)) + ((1./((d_y)^2))));


        p(i,j) = ((t_x+t_y)/denom);
    end
end

%pressure in region 3

for j=j_slit_2+1:j_max-1;
    for i=2:i_max-1;
         t_x = ((p(i+1,j))+(p(i-1,j)))/((d_x)^2);
         t_y = ((p(i,j+1))+(p(i,j-1)))/((d_y)^2);
         denom = (2.)*((1./((d_x)^2)) + ((1./((d_y)^2))));


         p(i,j) = ((t_x+t_y)/denom);
    end
end

%check convergence

error=0;
for j=2:j_max-1;
    for i= 2:i_max-1;
        error = (error + abs((p(i,j)-prev_p(i,j))))/(p_o);
    end
end
    error = error/(i_max-2)/(j_max-2)

%Calculation Q1 and Q3
Q1=0.0;
for i=2:i_max-1;
        Q1 = Q1+ (((4*(p(i,2)))-p(i,3))*d_x);

end

Q1= -(h^3)/(24*u)/d_y*Q1
```

```
Q3= Q1

%Calculation for Q2 and Q4
Q2=0.0;
for j=2:j_max-1;
        Q2 = Q2+ (((4*(p(2,j)))-p(3,j))*d_y);
end

Q2= -(h^3)/(24*u)/d_x*Q2
Q4= Q2

%Calculation total flow rate
Qt=Q1+Q2+Q3+Q4

%Calculation sill loads
sill_load1= 0.0;
for j=j_slit_1:j_slit_2;
   for i= 2:i_slit_1-1;
      sill_load1 = (sill_load1) + (p(i,j)* (d_x) * (d_y));
   end
end

sill_load2= 0.0;
for j=2:j_slit_1-1;
   for i=2:i_max-1;
      sill_load2 = (sill_load2) + (p(i,j)* (d_x) * (d_y));
  end
end

sill_load3= 0.0;
for j=j_slit_1:j_slit_2;
   for i= i_slit_2+1:i_max-1;
       sill_load3 = (sill_load3) + (p(i,j)* (d_x) * (d_y));
   end
end

sill_load4= 0.0;
for j=j_slit_2+1:j_max-1;
   for i=2:i_max-1;
      sill_load4 = (sill_load4) + (p(i,j)* (d_x) * (d_y));
   end

end

%Calculation recess load, total load and load coefficient
```

```
recess_load= p_o * l_r *  w_r

load= recess_load + sill_load1 +sill_load2 + sill_load3 + sill_load4

coefficient= load / recess_load

end
surf(p)
```

Appendix D

Finite Difference solutions for 2D case

Pressure varying in the y direction:

$$P_{i,j+1} = P_{i,\mathrm{j}} + \frac{\partial P_j}{\partial y}\Delta y + \frac{\partial^2 P_j}{\partial y^2}\frac{(\Delta y)^2}{2!} + \frac{\partial^3 P_j}{\partial y^3}\frac{(\Delta y)^3}{3!} + \cdots \qquad (11.1)$$

$$P_{i,j+2} = P_{i,j} + \frac{\partial P_j}{\partial y}(2\Delta y) + \frac{\partial^2 P_j}{\partial y^2}\frac{(2\Delta y)^2}{2!} + \frac{\partial^3 P_j}{\partial y^3}\frac{(2\Delta y)^3}{3!} + \cdots \qquad (11.2)$$

At a point, Δy is considered to be really small; and therefore, higher order term in the above equations are considered to be zero.

$$4\left(P_{i,j+1}\right) - P_{i,j+2} = 4P_{i,j} + \frac{\partial P_j}{\partial y}4\Delta y + \frac{\partial^2 P_j}{\partial y^2}2(\Delta y)^2 - P_{i,j} + \frac{\partial P_j}{\partial y}2\Delta y - \frac{\partial^2 P_j}{\partial y^2}2(\Delta \mathrm{y})^2 \quad (11.3)$$

Simplifying above equation:

$$\frac{\partial \mathrm{P_j}}{\partial \mathrm{y}} = \frac{4\left(\mathrm{P_{i,j+1}}\right) - \mathrm{P_{i,j+2}} - 3\left(\mathrm{P_{i,j}}\right)}{2\Delta \mathrm{y}} \qquad (11.4)$$

Pressure varying in the x direction:

$$\mathrm{P_{i+1,j}} = \mathrm{P_{i,j}} + \frac{\partial \mathrm{P_i}}{\partial \mathrm{x}}\Delta \mathrm{x} + \frac{\partial^2 \mathrm{P_i}}{\partial \mathrm{x}^2}\frac{(\Delta \mathrm{x})^2}{2!} + \frac{\partial^3 \mathrm{P_i}}{\partial \mathrm{x}^3}\frac{(\Delta \mathrm{x})^3}{3!} + \cdots \qquad (11.5)$$

$$\mathrm{P_{i,j+2}} = \mathrm{P_{i,j}} + \frac{\partial \mathrm{P_i}}{\partial \mathrm{x}}(2\Delta \mathrm{x}) + \frac{\partial^2 \mathrm{P_i}}{\partial \mathrm{x}^2}\frac{(2\Delta \mathrm{x})^2}{2!} + \frac{\partial^3 \mathrm{P_i}}{\partial \mathrm{x}^3}\frac{(2\Delta \mathrm{x})^3}{3!} + \cdots \qquad (11.6)$$

At a point, Δx is considered to be really small; and therefore, higher order terms in the above equations are considered to be zero.

$$4\left(\mathrm{P_{i+1,j}}\right) - \mathrm{P_{i+2,j}} = 4\mathrm{P_{i,j}} + \frac{\partial \mathrm{P_x}}{\partial \mathrm{x}}4\Delta \mathrm{x} + \frac{\partial^2 \mathrm{P_i}}{\partial \mathrm{x}^2}2(\Delta \mathrm{x})^2 - \mathrm{P_{i,j}} + \frac{\partial^2 \mathrm{P_i}}{\partial \mathrm{x}^2}2\Delta \mathrm{x} - \frac{\partial^3 \mathrm{P_i}}{\partial \mathrm{x}^3}2(\Delta \mathrm{x})^2 \quad (11.8)$$

Simplifying the Eq. (11.8):

$$\frac{\partial \mathrm{P_i}}{\partial \mathrm{x}} = \frac{4\left(\mathrm{P_{i+1,j}}\right) - \mathrm{P_{i+2,j}} - 3\left(\mathrm{P_{i,j}}\right)}{2\Delta \mathrm{x}} \qquad (11.9)$$

BIBLIOGRAPHY

Booser, E., & Khonsari, M. (2001). Applied Tribology: Bearing Design and Lubrication.

Fuller, D. (1956). Theory and Practice of Lubrication for Engineers.

Hamrock, J., Jacobson, B., & Schmid, S. (2004). Fundamentals of Fluid Film Lubrication.

ACADEMIC VITA

Judy Fan
1223 Banbury Circle, West Chester, PA 19380/ jywfan@gmail.com

Education and Training

The Pennsylvania State University **Expected to graduate in May, 2014**

- Schreyers Honors College
- Bachelor of Science in Mechanical Engineering
- Major Course Work:
  ME Design Methodology
  Vibration of Mechanical System
  Mechanical Design
  Instrumental Measurement and Statistics
  Fluid Flow

Presentation/Project

- MATLAB Application for Plane Stress Transformation Problems and Mohr's Circle. Presented at 2012 Sigma Xi Research Conference at Saint Joseph University, Philadelphia, Pa, April 2012
- Honors Thesis: Numerical Analysis on Bearing Lubrication
- Teach Kids Engineering Project
  -Build a free standing wind turbine model intended to teach kids engineering design and wind energy

Work Experience/Employment History

- **Tea Time** **University Park, PA,** Store Associate
  -Work at the register, making drinks and providing customer service
  January, 2013- Present
- **OfficeMax** **Exton, PA,** Sales Associates
  -In charge of providing great customer service and selling electronic products April, 2012- Present
- **Pennsylvania State University Library** **Media, PA.** Student Assistant
  -Assist students with technical difficulties and organize books
  Aug, 2010-May, 2012

Awards, Accomplishments and Achievements

- Dean's List Fall 2010-Spring 2012
  Fall 2013
- Delaware General Scholarship Fall 2011-Spring2012
- Academic Achievement Award Spring 2011&Spring2012
- Bonsall Trustee Scholarship For Schreyers Fall 2012- Spring 2013
- The Xerox Technical Minority Scholarship Fall 2012-Spring2013

Volunteer Experience

- Participate Canstruction in Philadelphia in 2011
  -Served as the Inventory Manager for the Canstruction team
- Fundraising for local schools with financial difficulties.

- Donate and fundraise for Ronald McDonald's at DuPont Hospital

Skills and Abilities

- Full proficiency in software such as Microsoft, Open Office and Google Docs
- Some experience with SolidWork
- Programming skill in MATLAB

Language Proficiency

- Advanced proficiency in Mandarin Chinese in both speaking and writing.